

The Evolution of Fluorescein into A Potential Theranostic Tool

Konstantinos S. Adamis,^[a] Michail Georgoulakis,^[a] Ioannis Angelonidis,^[a] Dimitris Korovesis,^[b] Christos Papadopoulos,^[a] Michael Kapsalis,^[a] Nektarios Tavernarakis,^[b, c] Nikolaos Eleftheriadis,^{*[a]} and Constantinos G. Neochoritis^{*[a]}

Recent advances in drug discovery and development have been marked by the emergence of new modalities, including small molecule theranostic agents. While initial results from clinical trials have been promising, modern detectable inhibitors are still in an early stage of development. In this study, we present a strategy for chemically evolving a fluorescent imaging agent into a potent therapeutic entity, which not only retains its properties but also enhances its inhibition and detection applicability. By utilizing 15-LOX-1 as a model system, we lever-

age prior knowledge of its inhibitors to rationally functionalize fluorescein, enabling the targeted and highly efficient synthesis of over 20 derivatives across four different scaffolds. This approach ultimately led to the development of a potent, cell-permeable inhibitor that effectively engages its target in live cells and enables real-time visualization. These findings validate our new strategy for the development of small molecule diagnostic modulators, paving the way for application in other targets as well.

1. Introduction

Drug discovery and development has experienced significant transformation in recent years, driven by the advent of novel chemotypes and the emergence of new therapeutic modalities.^[1] Researchers have broadened the drug toolbox in a determined effort to create the next generation of therapeutics focused on previously undruggable targets to address unmet medical needs.^[2] The development of more sophisticated approaches, including innovative drug delivery technologies, has led to a paradigm shift, resulting in a number of recent regulatory approvals for new types of medicine.^[3,4] Over the past five years, the traditional toolbox for drug discovery has expanded beyond conventional small molecules and biologics. New modalities, including bRo5 (beyond the rule of 5)

compounds such as RNA therapeutics, protein degraders, macrocycles, drug conjugates (i.e., antibody-drug and drug-drug conjugates, fluorescence-labeled drugs) and other multifunctional small molecules, have advanced significantly. These have shown clinical success and are now being considered early in the target evaluation process.^[5-7] An emerging modality with substantial potential are the small molecule theranostic agents,^[8,9] multifunctional entities that combine therapy and diagnostics in a single molecule in order to simultaneously treat and monitor disease progression, as well as assess response post-treatment.^[10] The diagnostic component identifies specific disease characteristics, while the therapeutic component treats the disease based on this information. The distinctive advantage of theranostics lies in their ability to both enable imaging and therapeutic intervention (aside other potential enhancements in drug delivery kinetics and efficacy).^[11-14] While traditional therapeutic agents lack diagnostic capabilities, commonly used bifunctional theranostics have not significantly advanced in drug development.^[15-18] This is largely due to their bifunctional design, which often leads to complex synthesis, low selectivity and reduced efficacy.^[19-22] With the rapid advancement of fluorescence microscopy and the widely acknowledged importance of small-molecule fluorescent probes in biological imaging, drug screening and medical diagnosis,^[23-28] developing a general workflow that leverages known molecules with one primary feature (either therapeutic or diagnostic) and rapidly fine-tuning them to develop the other feature, without adding a second moiety, could lead to theranostics with enhanced properties.

Herein, we showcase a strategy wherein a fluorescent imaging dye undergoes evolution into an efficient therapeutic entity, whilst maintaining, or even enhancing, its fluorescent properties (the term *evolved detectable inhibitor* or *EDI strategy* has been coined for this process, Figure 1). As opposed to strategies for developing traditional bifunctional fluorescent compound, such as activity and affinity-based chemical probes

[a] K. S. Adamis, M. Georgoulakis, I. Angelonidis, C. Papadopoulos, M. Kapsalis, Prof. N. Eleftheriadis, Prof. C. G. Neochoritis
Department of Chemistry, University of Crete, Voutes, Heraklion, Greece
E-mail: n.eleftheriadis@uoc.gr
kneochor@uoc.gr

[b] Dr. D. Korovesis, Prof. N. Tavernarakis
Foundation for Research and Technology Hellas, Institute of Molecular Biology and Biotechnology, Heraklion, Greece

[c] Prof. N. Tavernarakis
Division of Basic Sciences, School of Medicine, University of Crete, Voutes, Heraklion, Greece

Michail Georgoulakis, Ioannis Angelonidis, and Dimitris Korovesis contributed equally to this work.

Supporting information for this article is available on the WWW under <https://doi.org/10.1002/chem.202501513>

© 2025 The Author(s). Chemistry – A European Journal published by Wiley-VCH GmbH. This is an open access article under the terms of the Creative Commons Attribution-NonCommercial License, which permits use, distribution and reproduction in any medium, provided the original work is properly cited and is not used for commercial purposes.

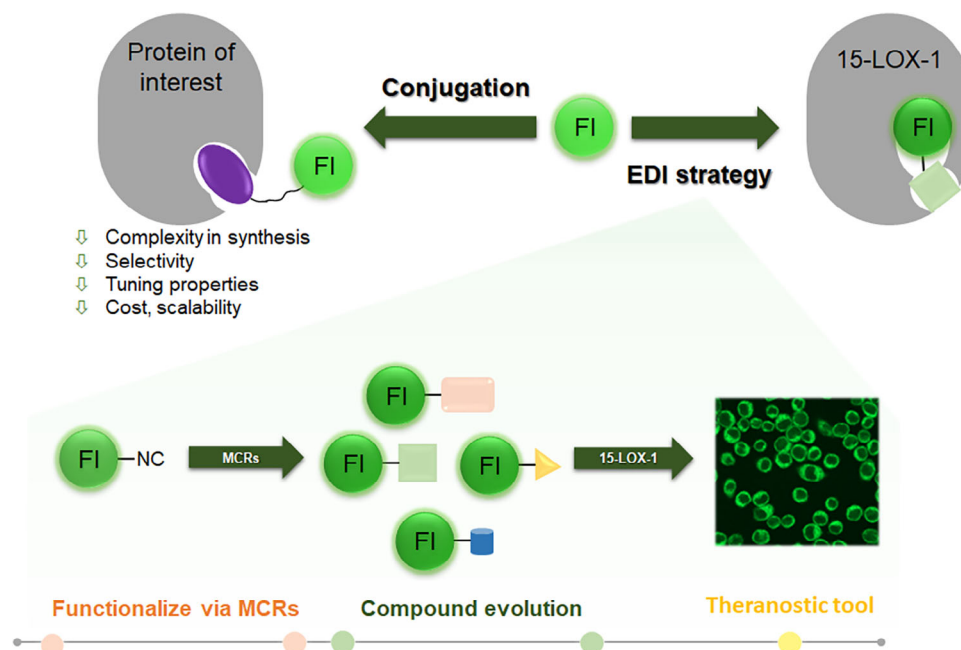


Figure 1. The workflow for our EDI strategy includes transforming an imaging agent, a suitably functionalized fluorescein (FI), into a potent theranostic tool in contrast to standard conjugation strategy with its drawbacks.

or photodynamic agents, we design an approach for rapidly and rationally functionalize fluorescein, an imaging agent, based on previous knowledge of inhibitors of the model protein human 15-lipoxygenase-1 (15-LOX-1). Our targeted one-step synthesis yielded more than 20 derivatives, spanning four different scaffolds, to ultimately leading to the identification of a potent, cell permeable, inherently fluorescent inhibitor that engages its target in live cells (Figure 1).

2. Results and Discussion

2.1. Exploitation of Our Strategy-Design

To exploit our strategy, we began with the well-known xanthene-based fluorophore fluorescein due to a variety of reasons; large molar extinction coefficient, high quantum yield and favorable solubility profile in water.^[29] In addition, fluorescein is already an FDA-approved drug (DB00693)^[30] and belongs to the WHO's list of essential medicines.^[31] A protein target in which, various xanthene and coumarin-based scaffolds have been reported as inhibitors is 15-LOX-1.^[32] This is a "double-edged sword" enzyme possessing a regulatory role in two pathways; it gives rise to inflammation and triggers apoptosis (ferroptosis). It has been implicated in high impact diseases like asthma, IBD, Alzheimer's, Parkinson's, leukemia and colon cancer.^[33–42] Therefore, fluorescein would serve as very good starting point for the development of an unprecedented theranostic tool.

We constructed an in-house virtual database of known xanthene and coumarin-based 15-LOX-1 inhibitors (>110) (Supporting Information, [.sdf file](#)). This database enabled the exploration of the key structural elements, substitution patterns and molecu-

lar features. A thorough analysis of all these inhibitors revealed an optimal specific substitution pattern on the core motif. Certain substitution patterns are more beneficial in terms of the inhibitors' efficacy, yielding more potent compounds (see, green and red dots, Figure 2A). Hence, we envisioned utilizing fluorescein as our main scaffold/hub with the appropriate substitution pattern (substitution of the C-3 position is a common element for all the inhibitors with an $IC_{50} < 10 \mu M$) to potentially fully occupy the enzyme's active site and explore possible novel interactions. It is noteworthy that a characteristic feature of xanthene-based fluorophores in general, and fluorescein in particular, is their pH sensitivity. Due to multiple complex equilibria, the ionic form of fluorescein exhibits much stronger fluorescence than the uncharged species. Fluorescein exists in equilibrium between a closed spirolactone form **1a** and an open form **1b** which is the fluorescent species; moreover, the external phenyl moiety at the 9-position should be kept out of the plane of the xanthene because it prevents quenching via a photo-induced transfer (PeT) mechanism (Figure 2B).^[43] Furthermore, electron donating groups on the phenyl group cause a significant decrease in quantum yield, whereas the phenolic oxygen seems to be important for fluorescence.^[15]

Multicomponent reaction (MCR) chemistry has become an established tool for molecular functionalization and for the exploration of uncharted chemical space. Due to its extremely convergent character, potential for diversification and, complexity enhancement and its effectiveness in the exploration of interactions with molecular targets,^[44–46] it has become a popular and highly effective tool for developing new modalities; including, functional chromophores and molecular probes.^[47–52]

Building on this, our objective was to primarily functionalize fluorescein, maintaining, or even enhancing, its fluorescent features, whilst, on the other hand and in parallel, rendering

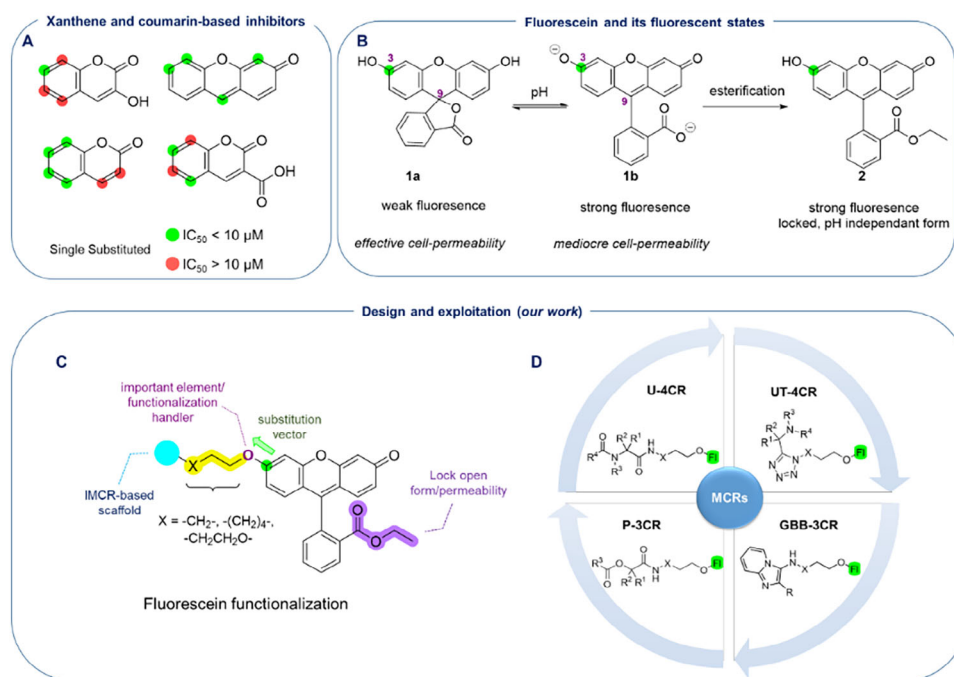


Figure 2. Designing our theranostics. (A) The substitution pattern on xanthene and coumarin-based inhibitors against 15-LOX-1. The green dots demonstrate potent inhibitors ($IC_{50} < 10 \mu M$), compared to the red ones ($IC_{50} > 10 \mu M$). (B) Functionalization of the fluorescein by locking it in its open form while maintaining the beneficial oxygen atom on the C-3 position. (C) Further functionalization of the fluorescein core through installation of an isocyanato group at the appropriate position. (D) Harnessing diverse IMCRs in order to rapidly and efficiently identify the first-in-class fluorescein-based inhibitor. The four scaffolds, derived from the different IMCRs, are shown.

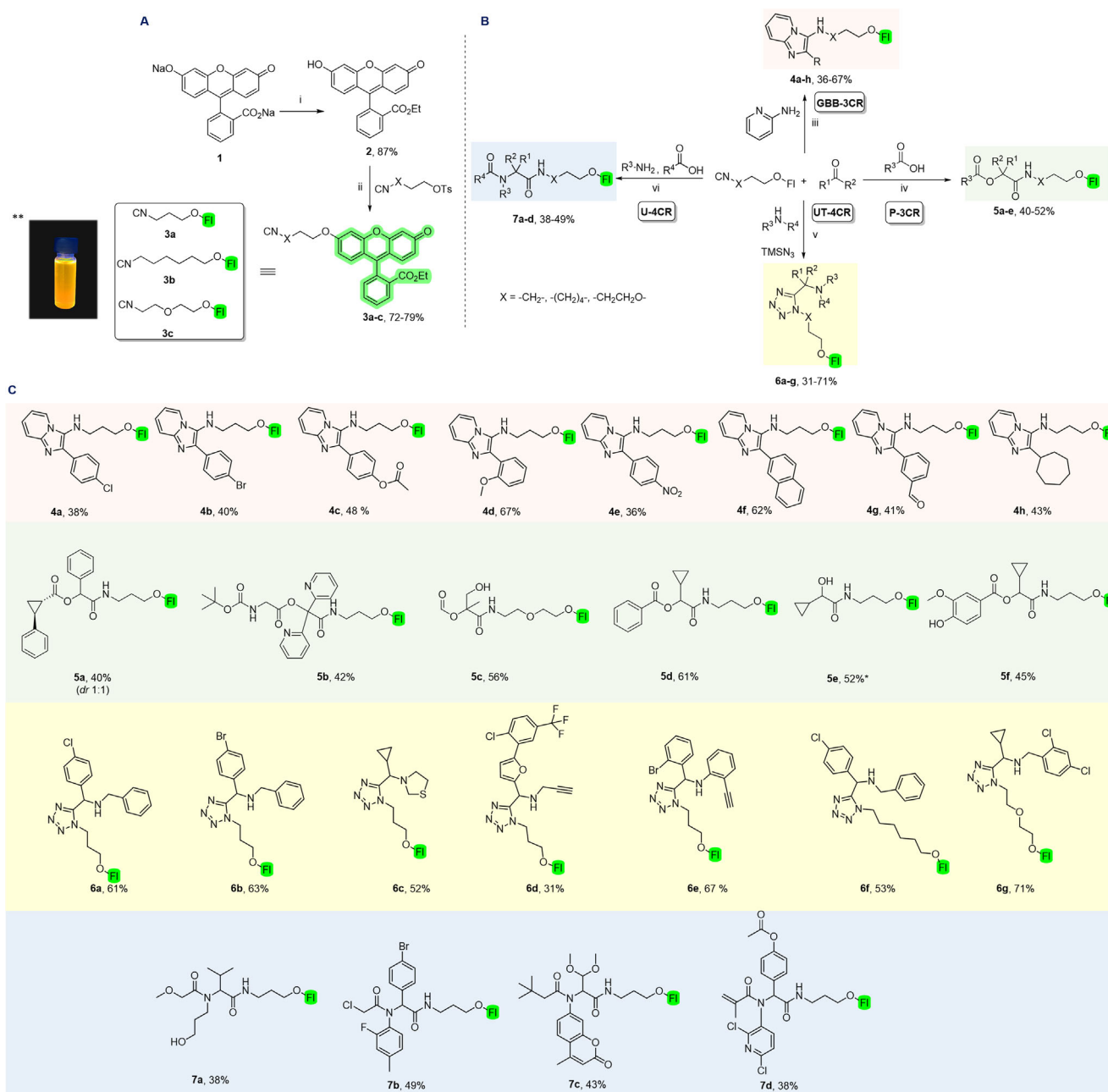
the molecule suitable for integration into the powerful MCR processes. Initially, fluorescein was locked in its open form by converting the carboxylate to the corresponding ethyl ester **2** using a simple and efficient method (Figure 2B). In so doing, we were able to maintain the required fluorescence in a pH-independent form, and, at the same time, we potentially improve the molecule's cell permeability due to the presence of the flexible ester moiety.^[53] Subsequently, we utilized linkers of varying lengths to install an isocyanide group at the C-3 position, facilitating the targeted isocyanide-based MCRs (IMCRs), without removing the important oxygen atom (Figure 2C). Isocyanides have garnered significant attention in biological applications due to their unique properties and distinctive reactivity, as well as their demonstrated ability to participate in biomolecule labeling.^[54–58]

In order to explore the chemical space in a more efficient manner and, taking into account all of the above regarding both fluorescein and the successful substitution pattern of the 15-LOX-1 inhibitors, we employed four different IMCRs; namely, the Ugi four-component (U-4CR),^[59] the Ugi tetrazole four-component (UT-4CR),^[60] the Passerini three-component (P-3CR)^[61] and the Groebke-Blackburn-Bienaymé three-component (GBB-3CR)^[62–64] reactions (Figure 2D). The choice of those MCRs was based on both the different chemical space that they cover with the distinct geometries and shapes of their products^[46] and the multitude of different functionalities and secondary transformations that we have explored for them in past.^[65–68] These features of our new strategy allowed us to rapidly identify and develop the first-in-class fluorescein-based inhibitors.

2.1.1. Synthesis

Accordingly, we performed an esterification reaction in dry EtOH with H_2SO_4 (Scheme 1A).^[69–71] The reaction was scalable (>25 mmol) and the targeted ethyl ester **2** could be isolated in 87% yield. Subsequently, utilizing the phenolic oxygen as a handle and in the presence of $NaHCO_3$, we successfully employed various isocyanotosylates of different sizes in order to install the versatile isocyanato group as part of a linker unit.^[66,72] 15-LOX-1 is an enzyme that binds extended linear molecules, due its natural substrates,^[73,74] so the linker unit in these molecules was expected to add affinity rather than just being a chemically necessary, but neutral addition. In this way, we successfully functionalized compound **2** furnishing the isocyanato-based derivatives **3a–c** in yields of 72–79% ready for the incorporation of fluorescein into the selected IMCRs to demonstrate the full scope of the proposed EDI strategy (Scheme 1A). Through our synthetic endeavors, we hoped to achieve as high diversity and complexity as possible in the product scaffolds (Scheme 1B).

The GBB-3CR has attracted tremendous attention over the last 5 years as indicated by the multitude of publications and patents centered on this reaction manifold.^[44,75] The GBB reaction, typically occurring between an aldehyde, an isocyanide and a 2-aminoheterocycle, affords imidazo[1,2-a]heterocycles, privileged scaffolds found in many drugs such as zolpidem, miroprofen, minodronic acid, olprinone and in many type-I kinase inhibitors.^[76] We obtained 8 different compounds in yields of 36–67%. The reaction has great scope with diverse aldehydes, both aromatic (with electron donating and withdrawing groups) and



Scheme 1. The synthetic overview of our approach and the libraries generated. (A) Functionalization of fluorescein and installation of the isocyno group; (i) dry EtOH, H₂SO₄, 24 h, 85 °C; (ii) NaHCO₃, DMF, 12 h, 80 °C; (B,C) The MCRs employed: GBB-3CR (pink box); P-3CR (green box); UT-4CR (yellow box); U-4CR (blue box) and their corresponding libraries; (iii) Sc(OTf)₃, MeOH, 45 °C, 24–72 h; (iv) DCM, rt, overnight; (v) MeOH, rt, 24–36 h; (vi) MeOH, rt, 24–48 h. (*Compound **5e** was obtained by the hydrolysis of **5f**. **Photo of the corresponding isocyanide **3a** was obtained by authors exhibiting the characteristic fluorescence (DMSO, 365 nm).)

aliphatic being suitable for inclusion. Interestingly, we obtained compound **4 g**, which bears an additional aldehyde group as a handle for further post-MCR modification, without the need for protection and deprotection steps (Scheme 1C). The P-3CR, in which an oxo-component, carboxylic acid and an isocyanide react together, yields very interesting α -acyloxy amides. Different carboxylic acids, even asymmetric ones, aldehydes and ketones, aliphatic and aromatics were utilized giving rise to adducts **5a-f** in yields of 40–52%. Particularly, in order to obtain an α -hydroxy amide, which would a) introduce metal chelating properties

(potentially targeting the iron in the enzyme's active site) and, b) enhance the physicochemical properties of our adducts (more soluble and linear molecules), we were able to perform a hydrolysis of the ester **5f**, toward the adduct **5e**, which can alternatively be accessed by a catalyzed P-2CR (Scheme 1C).^[77] The UT-4CR is a variation of the Ugi reaction which has been widely employed due to the fact that its 1,5-disubstituted tetrazole products serve as bioisosteres for carboxylic acids with improved metabolic stability and other advantageous physicochemical properties.^[45] The 7 different UT adducts (31–71%

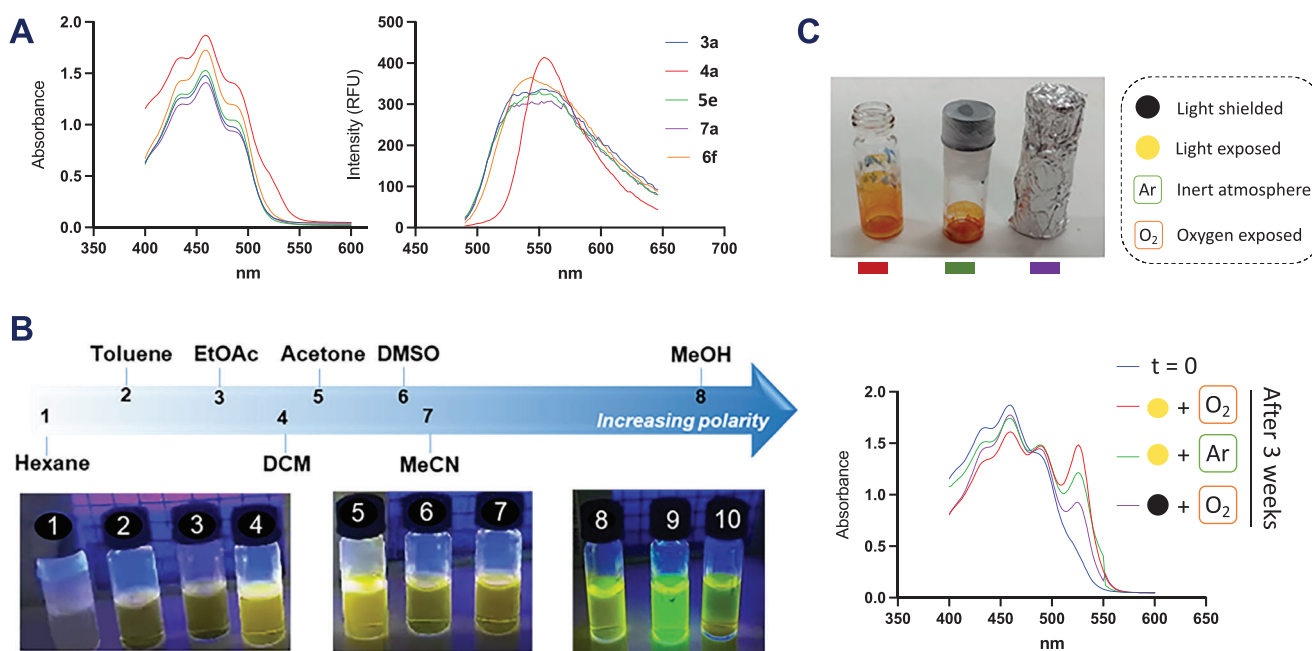


Figure 3. Characterization of the scaffolds 3–7. (A) Absorbance and emission spectra of representative derivatives. (B) The influence of solvent polarity on the fluorescence of compound 7a (365 nm): 8a, 9 and 10 correspond to MeOH, MeOH-HCl_(aq) and MeOH-Et₃N, respectively. (C) Stability experiments for compound 4a after 3 weeks exposure to different conditions (light/dark and ambient/inert atmosphere).

yield) demonstrate high diversity and complexity; both aromatic and aliphatic aldehydes and amines (primary and secondary) with a different substitution patterns work well. The reaction tolerates numerous functional groups, such as, cyclopropanes (i.e., 6c, 6g), triple bonds (i.e., 6d, 6e) and heterocycles (i.e., 6c, 6d). Once again, the chemistry provides opportunities for further post-MCR modifications, such as, C–C couplings via the terminal alkynes (i.e., 6d, 6e, Scheme 1C). The U-4CR is one of the most versatile reactions in synthetic chemistry as it gives rise to potentially very diverse α -acylamino acylamide adducts. In addition to the diversification points that it provides, the Ugi reaction very often serves as a hub for further ongoing orthogonal transformations. As such, the classical Ugi reaction has already been employed to access many commercially available drugs.^[78] Again, a strong focus for this sub-library was to access diversity in the products 7 (obtained in yields of 38–49% yield). A functional group tolerance was observed, with hydroxyl groups (i.e., 7a), a coumarin unit (i.e., 7c) and electrophilic warheads which could serve as potential proximity-inducing agents (i.e., 7b, 7d), all being readily incorporated, (Scheme 1C).^[79]

2.1.2. Physicochemical Characterization and Stability of the Products in the Synthesized Libraries

Next, we sought to characterize the physicochemical properties of the newly synthesized compounds. First, the absorbance and emission spectra for compounds 4–7 were obtained, showing similar profiles across all the different scaffolds (Figure 3A; see Supporting Information, Figure S1). The compounds display their maximum absorbance (λ_{max}) at 460 nm and fluorescence emission at 555 nm ($\lambda_{\text{ex}} = 460$ nm), with a Stoke shift ($\Delta\lambda$) of 95 nm. Comparing our findings with fluorescein 1, which presents an

excitation peak at 498 nm and an emission peak at 517 nm, we have accomplished a higher fluorescence wavelength, and, at the same time expanded the Stoke shift. Moreover, due to the appropriate solubility of our compounds, we examined the ability of different solvents to stabilize their excited state. Typically, a fluorophore has a larger dipole moment in the excited state (μ_{E}) than in the ground state and the solvent dipoles can reorient or relax around μ_{E} , which lowers the energy of the excited state. Compound 7a was dissolved in 8 different solvents, and, in line with the theory, as the solvent polarity increased, these effects more pronounced, resulting in emission at lower energies or longer wavelengths (Figure 3B). Finally, in order to assess the chemical stability of our compounds, we designed a three-week experiment, in which we evaluated the effect of exposure to light and/or ambient air. The majority of the compounds remained very stable, with the only exception being adducts 4 (from the GBB-3CR). Compound 4a was exposed to three sets of conditions for three weeks; light/ambient air, light/inert atmosphere, dark/ambient air. Afterwards, absorption and NMR spectra were taken, to determine the percentage of modified compound (Figure 3C; see Supporting Information, Figure S2). From our results, we conclude that both light and ambient air affect 4a, with the former being more significant (Figure 3C).

2.1.3. Inhibitory Studies of the Synthesized Library Adducts

Following on, we performed a preliminary evaluation of our newly synthesized derivatives against human 15-LOX-1, as described previously.^[73,74,80–83] After this initial inhibitory screening at 50 μM , and, in order to explore the precise inhibitory potency of all the active compounds, IC₅₀ values were determined.

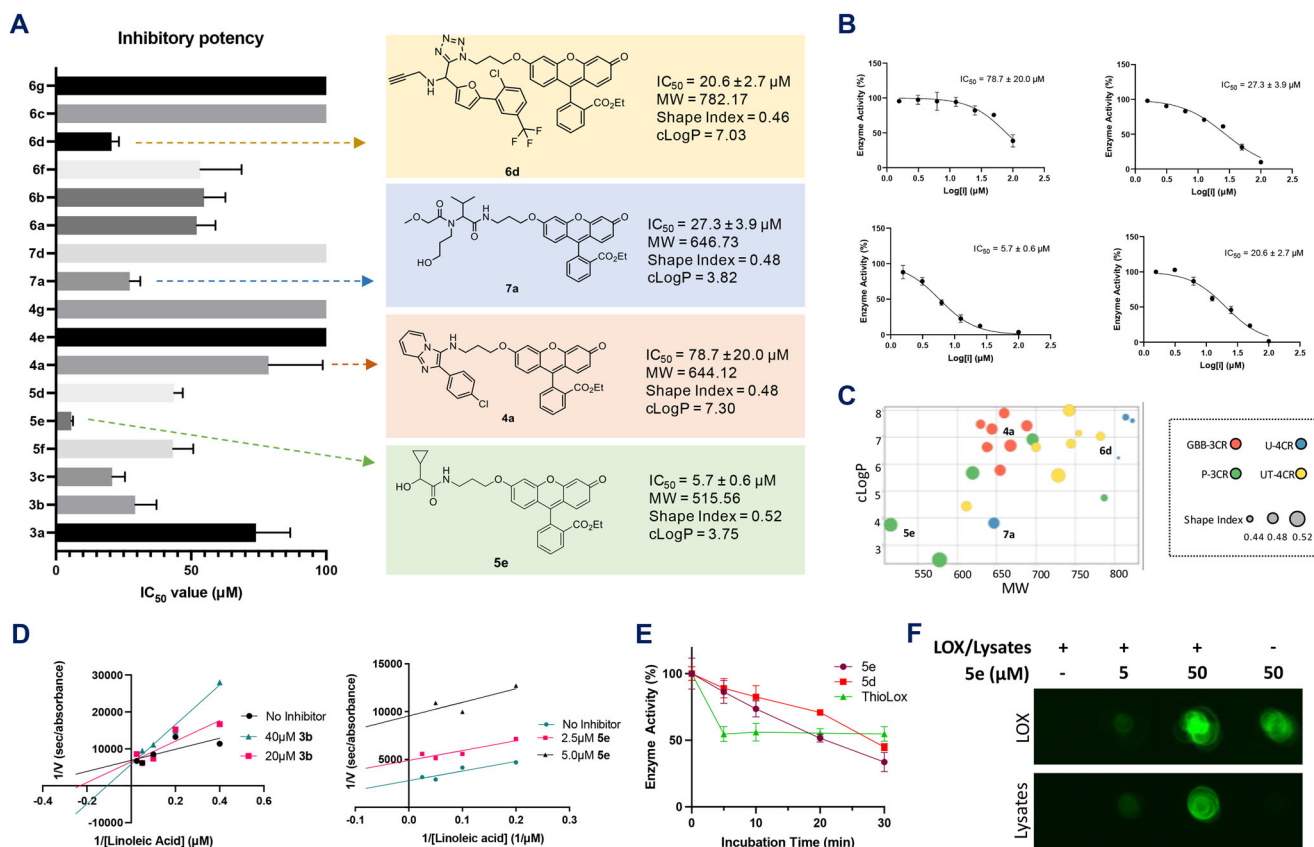


Figure 4. Inhibition studies of the synthesized derivatives. (A) Bar-graphs of the IC₅₀ activity of the synthesized derivatives against human 15-LOX-1. The most active compound per different MCR scaffold is presented along with its calculated properties (MW: Molecular Weight, Shape Index, cLogP); (B) IC₅₀ graphs for the compounds **6d**, **7a**, **4a** and **5e**; (C) 2D scatterplot of all the synthesized compounds based on lipophilicity (cLogP) and MW. The size and the color of every dot represents the shape index and the different MCR scaffold group, respectively; (D) Steady-state kinetic characterization of h-15-LOX-1 in the presence of different concentrations of the compounds **3b** and **5e** with Lineweaver – Burk representation; (E) Time-dependent inhibition assay in the presence of **5e**, **5d** and ThioLox. (F) Dot-blot (fluorescence) of **5e**-treated (5 and 50 μM) samples (pure 15-LOX-1 and cell lysate). Control experiments in the absence of **5e** is shown. All experiments were performed in triplicates ($n = 3$) and the standard error is reported.

We initially explored the influence of our modifications on the fluorescein scaffold, after esterification of the free acid and the introduction of the isocyanato groups with linkers of varying size. Interestingly, the ethyl ester **2** proved to be twice as potent (with the IC₅₀ value of 23.5 ± 3.8 μM) compared to the salt **1** (IC₅₀ = 44.8 ± 8.0 μM, Figure 4). The introduction of linkers with varying lengths onto **2** aimed to exploit the remaining available enzymatic pocket. Indeed, isocyanides **3a-c** exhibited increased inhibitory potency with the extension of linker length, aligning with our design goal of enhancing affinity through linker length, as 15-LOX-1 favors linear molecules (Figure 4). Recognizing the advantage of expansion in this direction and the available space in the pocket, we used the short linker (compound **3a**) to introduce various scaffolds. This strategy avoids the use of an aliphatic linker with suboptimal properties and limited interaction sites, facilitating the exploration of new scaffolds. Our objective is to develop compounds of similar size but with improved physicochemical properties and enhanced inhibitory potency. Compound **3a**, featuring a shorter linker and lower molecular weight, was selected for further functionalization to explore additional chemical space and improve the physicochemical and binding properties of the compounds.

By employing our EDI strategy, we have elegantly evolved our imaging agent to incorporate different scaffolds and to facilitate the study of structure-activity relationships (SARs). Our results nicely demonstrate a significant variation in the inhibitory activity dependent on the scaffold properties, which guides the correct orientation, and, as such, maximizes the contribution of the fluorescein group (Figure 4A-C). It is clear that properties such as MW, lipophilicity (cLogP) as well as molecular shape/complexity play a key role in optimum binding, and, therefore, in attaining better inhibitory potency. Specifically, the more compact GBB-3CR derivatives proved to be inactive against our model enzyme (Figure 4A-C; see Supporting Information, Figure S3), with the most potent compound (**4a**) exhibiting an IC₅₀ of 78.7 ± 20.0 μM (Figure 4B). The same is true for the branched (less linear, lower shape index) U-4CR derivatives and UT-4CR tetrazole derivatives (Figure 4A-C; see Supporting Information, Figure S3), with the best compounds **7a** and **6d** reaching an IC₅₀ of 27.3 ± 3.9 μM and IC₅₀ of 20.6 ± 2.7 μM, respectively (Figure 4). The most potent compound proved to be the P-3CR adduct **5e**, which, remarkably, exhibited an IC₅₀ of 5.7 ± 0.6 μM (Figure 4A,B). Notably, the noncleaved adduct **5f** exhibited a 8-fold lower inhibitory potency compared to **5e**, underscoring its potential role as a photocleavable precursor of

5e (Figure S2C). Compared to other adducts, **5e** is more linear (shape index = 0.52) and less lipophilic (cLogP = 3.75) with a small molecular weight (MW = 515.56, Figure 4C), which seems to possess many of the properties required for optimum binding. Once again, branched and bulky components on the P-3CR products yielded less active compounds (Figure 4A,C; see Supporting Information, Figure S3).

In order to investigate the binding mechanism of our compounds, we performed a Michaelis-Menten enzyme kinetics analysis of compounds **3a** and **5e**. As expected, **3a** showed competitive inhibition, as the Lineweaver-Burk plot indicates that the inhibitor causes an increase in the K_M values, whereas the V_{max} values remain constant (Figure 4D; see Supporting Information, Table S3). However, **5e** caused a decrease in both the K_M and V_{max} values (Figure 4D; see Supporting Information, Table S4), demonstrating an uncompetitive inhibition mechanism for 15-LOX-1. These findings indicate the possible involvement of the α -hydroxy amide warhead in the chelation of iron in the active site of 15-LOX-1, which, perhaps, enhances the inhibitory potency of **5e**.^[74] In order to explore this hypothesis, we performed molecular docking experiments, investigating the impact of iron on the number of binding site poses. Our results showed that compound **5e**, unlike **5d** and **3b**, exhibited a notable change in the number of docking poses within the enzyme's active site when Fe^{2+} or Fe^{3+} was present, compared to the absence of iron (Supporting Information, Figure S6).

This was confirmed by performing a time-dependent inhibition assay in the presence of **5e**, **5d**, and ThioLox^[82] (Figure 4E). In this experiment, the enzyme was incubated with the inhibitors for varying durations, ranging from 5 to 30 minutes, and the remaining enzyme activity was subsequently measured. We observed that only in the case of **5e** and **5d** there was a time-dependent inhibition, which was attributed to increased binding and iron chelation, followed by enzyme inactivation. In contrast, ThioLox, a known competitive inhibitor,^[82] reached a steady-state equilibrium within 5 minutes and exhibited the same inhibitory effect even after 30 minutes (Figure 4E).

Next, **5e** was utilized in labeling experiments with recombinant purified 15-LOX-1 and cell lysates (dot-blot experiments). Initially, **5e** (at concentrations of 5 μ M and 50 μ M) was incubated briefly with the purified enzyme, followed by acetone precipitation to remove unbound molecules. The results clearly showed that **5e** labeled 15-LOX-1, in contrast to the control experiments (Figure 4F). Similar results were observed when cell lysates (RAW 264.7 macrophage cells) were used, demonstrating the ability of **5e** to label the enzyme within a complex biological environment.

Finally, as similar α -hydroxy amide derivatives have been reported previously as chelating agents,^[84] we screened our compound against various pH conditions and a small library of different metals to evaluate its fluorescence stability. Showing remarkable stability in different pH (5–10 at 25 °C) and in presence of accumulated amounts of various metals, including Fe^{3+} , Ca^{2+} , Co^{2+} , Cu^{2+} , Mg^{2+} , Mn^{2+} and Zn^{2+} , we did not identify any significant quenching of fluorescence (Supporting Information, Figure S7).

Overall, compound **5e** combines a remarkable time dependent inhibitory potency with suitable physicochemical proper-

ties and fluorescence stability, and was, therefore, selected for further investigation in cell-based imaging studies.

2.1.4. In Cellulo Evaluation

In cellulo target engagement and labelling of 15-LOX-1 was investigated in a cell-based imaging assay using a confocal microscope. As opposed to a previously reported 15-LOX-1 biotinylated probe, the presence of the innate fluorescein core on **5e** should enable live-cell imaging as it does not require additional steps to visualize it (e.g., conjugation to labelled streptavidin post cell fixation). RAW 264.7 macrophage cells that express endogenous 15-LOX-1 were chosen as the model system, as previously.^[85,86]

Initially, we evaluated the cell permeability of **5e** by treating live cells (in situ, on the microscope) and immediately recording images to follow its cellular uptake. The fluorescence of **5e** could be distinguished from the background at concentrations as low as 50 nM (Supporting Information, Figure S8A,B). **5e** was taken up by the cells rapidly (within 1 minute) and reached saturation within 8 minutes (Figure 5A,B). Interestingly, fluorescein ester **2** was impermeable within the timeframe of our experiment (Supporting Information, Figure S9), suggesting that the α -hydroxy amide scaffold is highly beneficial for permeability, which verifies our design. While **5e** was distributed predominantly in the cytoplasm, some nuclear localization was also observed, albeit with a much lower signal (cell membrane labelling was negligible; Supporting Information, Figure S10). Nuclear localization was confirmed by co-staining with 4',6-diamidino-2-phenylindole (DAPI), post cell fixation (Supporting Information, Figure S10). Previously, the 15-LOX-1 biotinylated probe was shown to be evenly distributed between the cytoplasm and the nuclei of RAW 264.7, as well as to be colocalized with an antibody against 15-LOX-1.^[85] Consequently, the nuclear localization observed in our experiments may indicate nuclear labelling of 15-LOX-1. Given the differences in the labelling pattern between the two probes, we cannot rule out the possibility that **5e** does not efficiently cross the nuclear envelope. We note, however, that; i) visualization herein was done in live cells (as opposed to fixed cells, as required by the immunostaining experiments performed previously); and, ii) the uneven **5e** distribution is in agreement with a previous report directly visualizing 15-LOX-1 (GFP-fusion construct) in RAW 264.7 cells.^[87]

Next, we set out to evaluate whether the observed labelling by **5e** corresponds to 15-LOX-1 engagement in cells. To do so, we performed an imaging-based competition assay in live cells, using ThioLox as a competitor (Figure 5C).^[82] Given that ThioLox is a well-established potent 15-LOX-1 inhibitor, we expected that the **5e** signal would be reduced if labelling corresponds to 15-LOX-1 engagement, especially if this occurs in a dose-dependent manner. Initially, 5 μ M of **5e** was used in the competition assay, as this is close to its IC_{50} . While competition with an equimolar concentration of ThioLox ($IC_{50} \approx 12 \mu$ M) was not statistically significant, a 50% decrease in **5e** intensity was observed with when 10-times ThioLox concentration was used (Supporting Information, Figure S11). In order to explore if **5e** labelling could be reduced in dose-dependent manner (e.g., 10- and 100-times

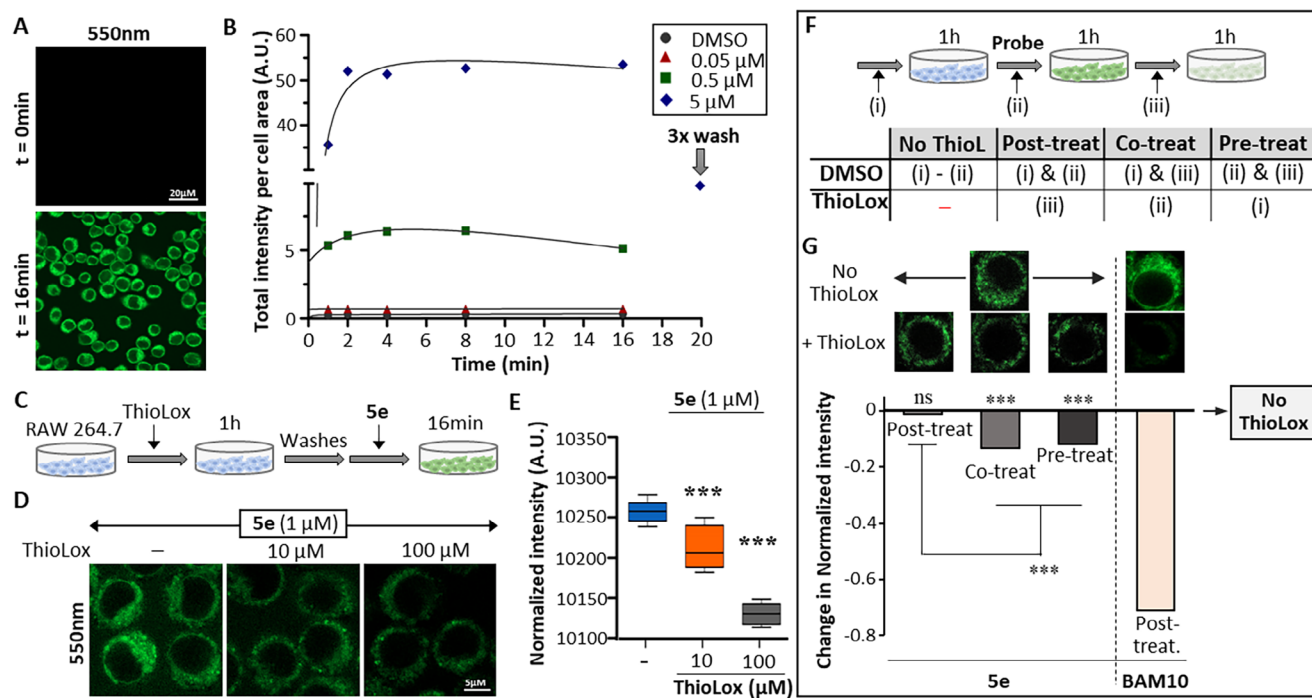


Figure 5. **5e** exhibits labeling of 15-LOX-1 in live cells consistent with irreversible interactions. (A) Imaging-based cell permeability assay using a confocal microscope. RAW 264.7 cells seeded on glass-bottom dishes were treated in situ with **5e** and immediately imaged. Top row shows cells prior to the treatment to obtain the background fluorescence. Bottom row shows an image of the cells 16 minutes after the addition of the 5 μM **5e** concentration. (B) Quantification of **5e** intensity in various time points show fast uptake of **5e**, which reaches saturation within 8 minutes. (C) Schematic representation of the imaging-based competition assay used for experiments shown in (D), (E), and Figure S11. **ThioLox** pre-treatment was performed at 37 °C, while **5e** labelling at room temperature. (D) Examples of images of live cells pre-treated with either DMSO (left image) or **ThioLox** (10 or 100 μM , middle and right, respectively) and subsequently labelled with 1 μM **5e**. (E) Box-plot of the quantified intensity per cell area from experiments using 1 μM **5e** with or without competition from **ThioLox**. **5e** intensity is reduced in dose-dependent manner in cells pre-treated with **ThioLox**; The box represents the interquartile range (25th to 75th percentile), the line inside the box represents the median, and the whiskers represent the minimum and maximum values. Data represent three independent experiments ($n = 3$). Statistical significance was assessed using a one-way ANOVA with Dunnett's multiple comparison test. Significance is indicated by stars (* $p < 0.05$, ** $p < 0.01$, *** $p < 0.001$). (F) Schematic representation of the imaging-based irreversibility assay used for experiments shown in (G) and Figure S12. All treatments were performed at 37 °C. (G) Diverging bar plot showing changes in normalized intensity for **5e** and **BAM10** under different conditions involving **ThioLox** as indicated in the table in (G). The line at zero represents the baseline condition (**5e** or **BAM10** – without **ThioLox** treatment), with bars indicating the change in intensity relative to this baseline. **5e** exhibits resistance to displacement in the post-treatment condition compared to co- and pre-treatment. When compared with **BAM10**, a recently covalent inhibitor developed by us,^[88] the data support the hypothesis that **5e** may act as an irreversible inhibitor. Data represent three independent experiments ($n = 3$). Statistical significance was assessed using Welch's t-test (t-test assuming unequal variances). Significance is indicated by stars (* $p < 0.05$, ** $p < 0.01$, *** $p < 0.001$).

concentrations) by **ThioLox**, we repeated the experiments using 1 μM of **5e** so that **ThioLox** solubility was not the limiting factor. Indeed, we observed that labelling by **5e** was reduced in a dose-dependent manner by **ThioLox** (Figure 5D,E). These results indicate that **5e** labeling is 15-LOX-1-dependent, reflecting specific and robust binding.

Finally, we sought to explore in cells whether the observed behavior of **5e** on purified 15-LOX-1 supports an irreversible mechanism. For that, we employed a cell-based irreversibility assay recently used to demonstrate the *in cellulo* irreversible mechanism of a novel probe developed by us that utilizes the established bis-alkyne 15-LOX-1-specific covalent warhead (Figure 5F, "Post-treat" condition).^[88] In this assay, cells are incubated with the probe followed by treatment with **ThioLox** and it is designed to evaluate whether binding of a probe is resistant to competitive displacement. Under this condition, **5e** labelling showed virtually no reduction in normalized fluorescence intensity (Figure 5G, "Post-treat" bar). In comparison, **BAM10**, our recently reported covalent binder,^[88] which is exhibited a

measurable reduction in fluorescence intensity under the same conditions (Figure 5G, last bar). These findings suggest that **5e** exhibits strong resistance to displacement from the enzyme's active site and, most importantly, induces prolonged enzyme inactivation, highlighting its potential theranostic capability. Further validation through co- and pre-treatment experiments revealed that **5e** could be displaced by **ThioLox** in the same experimental setup, as indicated by significant reductions in fluorescence intensity (Figure 5G, "Co-treat" and "Pre-treat" bars). The stark contrast between the post-treatment condition, where displacement was absent, and the co- and pre-treatment conditions, coupled with the comparison to **BAM10**, strongly supports the hypothesis that **5e** binds to 15-LOX-1 in live cells through an irreversible mechanism.

Overall, our experiments demonstrate that **5e** is a cell-permeable 15-LOX-1 inhibitor that specifically engages its target in live cells, providing valuable insights into its target engagement and cellular localization. Furthermore, the resistance of **5e** to competitive displacement in our irreversibility assay

supports the hypothesis that **5e** operates through a novel covalent binding mechanism.

3. Conclusion

In conclusion, our study demonstrates the successful evolution of a fluorescent imaging agent into a potent therapeutic compound. By functionalizing fluorescein, we have not only enhanced its fluorescent properties, but also rendered it suitable for integration into the multicomponent reaction (MCR) framework. We have developed > 20 compounds representing four different scaffolds with diverse and distinct geometries and shape. Compound **5e** exhibits strong time-dependent inhibitory potency against 15-LOX-1, along with favorable physicochemical properties and stable fluorescence. These features enable successful in vitro enzyme labeling and make it well-suited for further investigation. Additionally, its ability to permeate the cell membrane, engage its target in live cells, and cause prolonged enzyme inactivation underscores its potential as a theranostic agent for cell-based imaging studies. We foresee that the described strategy could be more generally applied to the development of small molecule imaging agents with inhibitory applications in drug discovery.

Supporting Information

Synthetic procedures, ^1H , ^{13}C NMR and HRMS analytical data, for the synthesized compounds, absorption-fluorescence measurements, expression and purification of 15-LOX-1, enzyme inhibition studies, determination of the half maximal inhibitor concentration (IC_{50}), metal screening, general methods for cell and imaging studies. The authors have cited additional references within the [Supporting Information](#).^[1–8]

Acknowledgements

The authors acknowledge the Empeirikeion Foundation, the National Recovery and Resilience Plan Greece 2.0, funded by the European Union-NextGenerationEU (project code: TAEDR-0535850), and the Hellenic Foundation for Research and Innovation (H.F.R.I.) under the Greece 2.0 Basic Research Financing Action «Horizontal support of all sciences» Sub-action 2 (project number: 15511), 2nd Call for H.F.R.I. Research Projects to support Post-Doctoral Researchers (Project Number: 0911) and University of Crete (ELKE) for providing grants to N.E and C.G.N. Work in N.T.'s laboratory is funded by grants from the Hellenic Foundation for Research and Innovation (HFRI-FM17C3-0869, NeuroMitophagy) and the General Secretariat for Research and Innovation of the Greek Ministry of Development and Investments. D.K. is supported by European Research Area (ERA) Postdoctoral Fellowship under Marie Skłodowska-Curie Actions (UnFearHD-Grant agreement ID: 101130833). The authors would also like to sincerely

thank Dr. Tamsyn Montagnon for her valuable remarks and the mass spectrometry facility of the University of Crete.

Conflict of Interests

The authors declare no conflict of interest.

Data Availability Statement

The data that support the findings of this study are available from the corresponding author upon reasonable request.

Keywords: 15-LOX-1 · fluorescein · fluorescence · multicomponent reactions · theranostics

- [1] Y. Choi, A. A. Vinks, P. H. van der Graaf, *Clin. Pharmacol. Ther.* **2023**, *114*, 493.
- [2] E. C. Scott, A. C. Baines, Y. Gong, R. Moore, G. E. Pamuk, H. Saber, A. Subedee, M. D. Thompson, W. Xiao, R. Pazdur, V. A. Rao, J. Schneider, J. A. Beaver, *Nat. Rev. Drug Discov.* **2023**, *22*, 625.
- [3] M.-J. Blanco, in *Drug Discovery and Evaluation: Safety and Pharmacokinetic Assays*, Springer International Publishing, Cham **2023**, pp. 1.
- [4] Y. P. Auberson, P. B. Arimondo, M. Duca, S. Essig, U. Grether, A. C. Rufer, G. Sbardella, U. Schopfer, A. Torrens, M. van der Stelt, B. Vauzeilles, O. Vázquez, A. X. Zhang, *ChemBioChem* **2023**, *24*, 1.
- [5] M.-J. Blanco, K. M. Gardinier, *ACS Med. Chem. Lett.* **2020**, *11*, 228.
- [6] J. Aubé, C. W. Lindsley, C. E. Müller, *J. Med. Chem.* **2023**, *66*, 7669.
- [7] E. Valeur, S. M. Guéret, H. Adihou, R. Gopalakrishnan, M. Lemurell, H. Waldmann, T. N. Grossmann, A. T. Plowright, *Angew. Chem. – Int. Ed.* **2017**, *56*, 10294.
- [8] S. S. Kelkar, T. M. Reineke, *Bioconjug Chem.* **2011**, *22*, 1879.
- [9] G. B. Bilgin, C. Bilgin, B. J. Burkett, J. J. Orme, D. S. Childs, M. P. Thorpe, T. R. Halfdanarson, G. B. Johnson, A. T. Kendi, O. Sartor, *Theranostics* **2024**, *14*, 2367.
- [10] S. Pratihari, K. K. Bhagavath, T. Govindaraju, *RSC Chem. Biol.* **2023**, *4*, 826.
- [11] A. Corlett, J.-A. Pinson, M. N. Rahimi, J. Van Zuylekom, C. Cullinane, B. Blyth, P. E. Thompson, C. A. Hutton, P. D. Roselt, M. B. Haskali, *J. Med. Chem.* **2023**, *66*, 10289.
- [12] M. L. Bolognesi, A. Gandini, F. Prati, E. Uliassi, *J. Med. Chem.* **2016**, *59*, 7759.
- [13] Y. Song, J. Zou, E. A. Castellanos, N. Matsuura, J. A. Ronald, A. Shuhendler, W. A. Weber, A. A. Gilad, C. Müller, T. H. Witney, X. Chen, *Theranostics* **2024**, *14*, 2464.
- [14] S. H. Sinha, E. A. Owens, Y. Feng, Y. Yang, Y. Xie, Y. Tu, M. Henary, Y. G. Zheng, *Eur. J. Med. Chem.* **2012**, *54*, 647.
- [15] K. Colas, S. Doloczi, M. Posada Urrutia, C. Dyrager, *Eur. J. Org. Chem.* **2021**, *2021*, 2133.
- [16] S. B. Wagh, V. A. Maslivet, J. J. La Clair, A. Kornienko, *ChemBioChem* **2021**, *22*, 3109.
- [17] S. Zeng, X. Liu, Y. S. Kafuti, H. Kim, J. Wang, X. Peng, H. Li, J. Yoon, *Chem. Soc. Rev.* **2023**, *52*, 5607.
- [18] K. Kawai, T. Hirayama, H. Imai, T. Murakami, M. Inden, I. Hozumi, H. Nagasawa, *J. Am. Chem. Soc.* **2022**, *144*, 3793.
- [19] M. Minoshima, S. I. Reja, R. Hashimoto, K. Iijima, K. Kikuchi, *Chem. Rev.* **2024**, *124*, 6198.
- [20] A. J. van der Zouwen, M. D. Witte, *Front. Chem.* **2021**, *9*, 1.
- [21] E. I. Vrettos, S. G. Kyrkou, V. Zoi, M. Giannakopoulou, M. V. Chatziathanasiadou, Z. Kanaki, A. Agalou, V. Bistas, A. Kouglioumtzi, T. Karampelas, D. A. Diamantis, C. Murphy, D. Beis, A. Klinakis, C. Tamvakopoulos, A. P. Kyritsis, G. A. Alexiou, A. G. Tzakos, *Chem. Eur. J.* **2024**, *30*, e202401327.
- [22] S. M. Usama, B. Zhao, K. Burgess, *Chem. Soc. Rev.* **2021**, *50*, 9794.
- [23] D. Seah, Z. Cheng, M. Vendrell, *ACS Nano* **2023**, *17*, 19478.

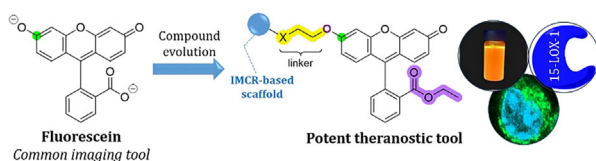
- [24] A. S. Klymchenko, *Acc. Chem. Res.* **2023**, *56*, 1.
- [25] K. Fujita, Y. Urano, *Chem. Rev.* **2024**, *124*, 4021.
- [26] X. Wang, Q. Ding, R. R. Groleau, L. Wu, Y. Mao, F. Che, O. Kotova, E. M. Scanlan, S. E. Lewis, P. Li, B. Tang, T. D. James, T. Gunnlaugsson, *Chem. Rev.* **2024**, *124*, 7106.
- [27] H. Chang, S. Clemens, P. Gao, Q. Li, H. Zhao, L. Wang, J. Zhang, P. Zhou, K. Johnsson, L. Wang, *J. Am. Chem. Soc.* **2024**, *146*, 20569.
- [28] Y. Urano, M. Kamiya, K. Kanda, T. Ueno, K. Hirose, T. Nagano, *J. Am. Chem. Soc.* **2005**, *127*, 4888.
- [29] M. Beija, C. A. M. Afonso, J. M. G. Martinho, *Chem. Soc. Rev.* **2009**, *38*, 2410.
- [30] C. Knox, M. Wilson, C. M. Klinger, M. Franklin, E. Oler, A. Wilson, A. Pon, J. Cox, N. E. Lucy Chin, S. A. Strawbridge, M. Garcia-Patino, R. Kruger, A. Sivakumaran, S. Sanford, R. Doshi, N. Khetarpal, O. Fatokun, D. Doucet, A. Zubkowski, D. Y. Rayat, H. Jackson, K. Harford, A. Anjum, M. Zakir, F. Wang, S. Tian, B. Lee, J. Liigand, H. Peters, R. Q. Rachel Wang, et al., *Nucleic Acids Res.* **2024**, *52*, D1265.
- [31] World Health Organization, *World Health Organization Model List of Essential Medicines: 21st List 2019*, World Health Organization, Geneva PP – Geneva, **2019**, n.d.
- [32] H. Sadeghian, A. Jabbari, *Expert Opin. Ther. Pat.* **2016**, *26*, 65.
- [33] B. Samuelsson, S. Dahlen, J. A. N. A. Lindgren, C. A. Rouzer, C. N. Serhan, *Science* **1987**, *237*, 1171.
- [34] J. Z. Haeggström, C. D. Funk, *Chem. Rev.* **2011**, *111*, 5866.
- [35] F. Mao, Y. Wu, X. Tang, J. Wang, Z. Pan, P. Zhang, B. Zhang, Y. Yan, X. Zhang, H. Qian, W. Xu, *Biotechnol. Lett.* **2017**, *39*, 929.
- [36] J. Zhao, V. B. O'Donnell, S. Balzar, C. M. St Croix, J. B. Trudeau, S. E. Wenzel, *Proc. Natl. Acad. Sci. USA* **2011**, *108*, 14246.
- [37] U. Mabalirajan, R. Rehman, T. Ahmad, S. Kumar, G. D. Leishangthem, S. Singh, A. K. Dinda, S. Biswal, A. Agrawal, B. Ghosh, *Sci. Rep.* **2013**, *3*, 1540.
- [38] Y. B. Joshi, P. F. Giannopoulos, D. Praticò, *Trends Pharmacol. Sci.* **2015**, *36*, 181.
- [39] K. van Leyen, K. Arai, G. Jin, V. Kenyon, B. Gerstner, P. A. Rosenberg, T. R. Holman, E. H. Lo, *J. Neurosci. Res.* **2008**, *86*, 904.
- [40] A. J. Klil-Drori, A. Ariel, *Prostaglandins Other Lipid Mediat.* **2013**, *106*, 16.
- [41] M. A. Vaezi, B. Safizadeh, A. R. Eghtedari, S. S. Ghorbanhosseini, M. Rastegar, V. Salimi, M. Tavakoli-Yaraki, *Lipids Health Dis.* **2021**, *20*, 169.
- [42] H.-E. Claesson, W. J. Griffiths, Å. Brunnström, F. Schain, E. Andersson, S. Feltenmark, H. A. Johnson, A. Porwit, J. Sjöberg, M. Björkholm, *FEBS J.* **2008**, *275*, 4222.
- [43] T. Miura, Y. Urano, K. Tanaka, T. Nagano, K. Ohkubo, S. Fukuzumi, *J. Am. Chem. Soc.* **2003**, *125*, 8666.
- [44] A. Boltjes, A. Dömling, *Eur. J. Org. Chem.* **2019**, 7007.
- [45] C. G. Neochoritis, T. Zhao, A. Dömling, *Chem. Rev.* **2019**, *119*, 1970.
- [46] A. Dömling, W. Wang, K. Wang, *Chem. Rev.* **2012**, *112*, 3083.
- [47] R. O. Rocha, M. O. Rodrigues, B. A. D. Neto, *ACS Omega* **2020**, *5*, 972.
- [48] T. Kambe, B. E. Correia, M. J. Niphakis, B. F. Cravatt, *J. Am. Chem. Soc.* **2014**, *136*, 10777.
- [49] L. Zhang, M. Isselstein, J. Köhler, N. Eleftheriadis, N. M. Huisjes, M. Guirao-Ortiz, A. Narducci, J. H. Smit, J. Stoffels, H. Harz, H. Leonhardt, A. Herrmann, T. Cordes, *Angew. Chem. – Int. Ed.* **2022**, *61*, e202112959.
- [50] J. Ge, X. Cheng, L. P. Tan, S. Q. Yao, *Chem. Commun.* **2012**, *48*, 4453.
- [51] J. S. Cisar, B. F. Cravatt, *J. Am. Chem. Soc.* **2012**, *134*, 10385.
- [52] L. Zhang, C. Wang, Y. Li, H. Wang, K. Sun, S. Lu, Y. Wang, S. Jing, T. Cordes, *Angew. Chem., Int. Ed.* **2025**, *64*, e202415627.
- [53] L. Wang, M. Tran, E. D'Este, J. Roberti, B. Koch, L. Xue, K. Johnsson, *Nat. Chem.* **2020**, *12*, 165.
- [54] J. Tu, M. Xu, S. Parvez, R. T. Peterson, R. M. Franzini, *J. Am. Chem. Soc.* **2018**, *140*, 8410.
- [55] R. J. B. Schäfer, M. R. Monaco, M. Li, A. Tirla, P. Rivera-Fuentes, H. Wennemers, *J. Am. Chem. Soc.* **2019**, *141*, 18644.
- [56] Y. Zhu, J.-Y. Liao, L. Qian, *Front. Chem.* **2021**, *9*, 670751.
- [57] P. Patil, Q. Zheng, K. Kurpiewska, A. Dömling, *Nat. Commun.* **2023**, *14*, 5807.
- [58] A. Geißler, H. Junca, A. M. Kany, L. J. Daumann, A. K. H. Hirsch, D. H. Pieper, S. A. Sieber, *Chem. Sci.* **2024**, *15*, 11946.
- [59] I. Ugi, C. Steinbrückner, DE-B, *1*, 103, 337, **1959**.
- [60] I. Ugi, R. Meyr, *Chem. Ber.* **1961**, *94*, 2229.
- [61] M. Passerini, *Gazz. Chim. Ital.* **1921**, *51*, 126.
- [62] K. Groebke, L. Weber, F. Mehlin, *Synlett* **1998**, 661.
- [63] C. Blackburn, B. Guan, P. Fleming, K. Shiosaki, S. Tsai, *Tetrahedron Lett.* **1998**, *39*, 3635.
- [64] H. Bienaymé, K. Bouzid, *Angew. Chem., Int. Ed.* **1998**, *37*, 2234.
- [65] M. Fragkiadakis, P.-K. Anastasiou, I. Volyrakis, A. Pantousas, C. C. Stoumpos, C. G. Neochoritis, *Chem. Commun.* **2023**, *59*, 14411.
- [66] M. Fragkiadakis, P. Anastasiou, M. Zingiridis, M. E. Triantafyllou-Rundell, A. R. Romero, C. C. Stoumpos, C. G. Neochoritis, *J. Org. Chem.* **2023**, *88*, 12709.
- [67] X. Lei, P. Lampiri, P. Patil, G. Angeli, C. G. Neochoritis, A. Dömling, *Chem. Commun.* **2021**, *57*, 6652.
- [68] X. Lei, G. K. Angeli, C. G. Neochoritis, A. Dömling, *Green Chem.* **2022**, *24*, 6168.
- [69] M. Adamczyk, J. Grote, *Tetrahedron Lett.* **2000**, *41*, 807.
- [70] F. Schubert, D. Cech, R. Reinhardt, P. Wiesner, *DNA Sequence* **1992**, *2*, 273.
- [71] W. Feuerstein, M. Dutoit, *Ber. Dtsch. Chem. Ges.* **1901**, *34*, 2637.
- [72] I. P. Bhela, A. Ranza, F. C. Balestrero, M. Serafini, S. Aprile, R. M. C. Di Martino, F. Condorelli, T. Pirali, *J. Med. Chem.* **2022**, *65*, 15282.
- [73] N. Eleftheriadis, C. G. Neochoritis, N. G. J. Leus, P. E. van der Wouden, A. Dömling, F. J. Dekker, *J. Med. Chem.* **2015**, *58*, 7850.
- [74] N. Spacho, M. Casertano, C. Imperatore, C. Papadopoulos, M. Menna, N. Eleftheriadis, *Chem. Eur. J.* **2024**, *30*, e202402279.
- [75] C. Martini, M. I. D. Mardjan, A. Basso, *Beilstein J. Org. Chem.* **2024**, *20*, 1839.
- [76] M. Konstantinidou, Z. Boiarska, R. Butera, C. G. Neochoritis, K. Kurpiewska, J. Kalinowska-Tluscik, A. Dömling, *Eur. J. Org. Chem.* **2020**, 5601.
- [77] S. E. Denmark, Y. Fan, *J. Am. Chem. Soc.* **2003**, *125*, 7825.
- [78] E. Fotopoulou, P. K. Anastasiou, C. Tomza, C. G. Neochoritis, *Tetrahedron Green Chem.* **2024**, *3*, 100044.
- [79] F. Sutanto, S. Shaabani, C. G. Neochoritis, T. Zarganes-Tzitzikas, P. Patil, E. Ghonchepour, A. Dömling, *Sci. Adv.* **2021**, *7*, eabd9307.
- [80] N. Eleftheriadis, S. A. Thee, M. R. H. Zwinderman, N. G. J. Leus, F. J. Dekker, *Angew. Chem. – Int. Ed.* **2016**, *55*, 12300.
- [81] N. Eleftheriadis, S. Thee, J. te Biesebeek, P. van der Wouden, B.-J. J. Baas, F. J. Dekker, *Eur. J. Med. Chem.* **2015**, *94*, 265.
- [82] N. Eleftheriadis, H. Poelman, N. G. J. Leus, B. Honrath, C. G. Neochoritis, A. Dolga, A. Dömling, F. J. Dekker, *Eur. J. Med. Chem.* **2016**, *122*, 786.
- [83] R. van der Vlag, H. Guo, U. Hapko, N. Eleftheriadis, L. Monjas, F. J. Dekker, A. K. H. Hirsch, *Eur. J. Med. Chem.* **2019**, *174*, 45–55.
- [84] H. Sayre, K. Milos, M. J. Goldcamp, C. A. Schroll, J. A. Krause, M. J. Baldwin, *Inorg. Chem.* **2010**, *49*, 4433.
- [85] D. Chen, Z. Xiao, H. Guo, D. Gogishvili, R. Setroikromo, P. E. van der Wouden, F. J. Dekker, *Angew. Chem., Int. Ed.* **2021**, *60*, 21875.
- [86] H. Guo, I. C. Verhoeck, G. H. Prins, R. van der Vlag, P. E. van der Wouden, R. van Merkerk, W. J. Quax, P. Olinga, A. K. H. Hirsch, F. J. Dekker, *J. Med. Chem.* **2019**, *62*, 4624.
- [87] P. Christmas, J. W. Fox, S. R. Ursino, R. J. Soberman, *J. Biol. Chem.* **1999**, *274*, 25594.
- [88] A. Louka, N. Spacho, D. Korovesis, K. Adamis, C. Papadopoulos, E. Kalaitzaki, N. Tavernarakis, C. G. Neochoritis, N. Eleftheriadis, *Angew. Chem., Int. Ed.* **2024**, e202418291.

Manuscript received: April 22, 2025

Revised manuscript received: April 30, 2025

Version of record online: ■■■

RESEARCH ARTICLE



Our study successfully evolved a fluorescent imaging agent into a potent therapeutic compound. By functionalizing fluorescein, we enhanced its fluorescence and adapted it for multicomponent reactions (MCRs). We

synthesized over 20 compounds across four diverse scaffolds. Compound **5e** shows strong 15-LOX-1 inhibition, favorable properties and cell permeability, making it ideal for imaging and screening assays.

K. S. Adamis, M. Georgoulakis, I. Angelonidis, D. Korovesis, C. Papadopoulos, M. Kapsalis, N. Tavernarakis, N. Eleftheriadis, C. G. Neochoritis

1 – 10

The Evolution of Fluorescein into A Potential Theranostic Tool

